

Seismic structural health monitoring using the modal assurance distribution

Said Quqa  | Luca Landi  | Pier Paolo Diotallevi 

Department of Civil, Chemical, Environmental, and Materials Engineering, University of Bologna, Bologna, Italy

Correspondence

Said Quqa, Department of Civil, Chemical, Environmental, and Materials Engineering, University of Bologna, Viale del Risorgimento 2, Bologna 40136, Italy.
Email: said.quqa2@unibo.it

Abstract

Thanks to emerging techniques in the field of signal processing and due to improvements in smart sensing systems which enable the event-triggered acquisition of high-fidelity data at the occurrence of strong ground motion events, seismic structural health monitoring has grown considerably in the last few decades. In this paper, the modal assurance distribution, an alternative time-frequency representation of the modal features of multivariate and multicomponent signals, is extended for application to short-term nonstationary vibrational structural responses in which the system may manifest its nonlinear behavior. A general procedure for the extraction of the decoupled normal modes is presented, which allows the identification of instantaneous modal parameters in order to investigate in detail the structural behavior during earthquakes. Valuable information that cannot be recovered by means of traditional criteria can thus be exploited for accurate damage assessment. The results obtained for two case studies consisting of a numerical model with softening nonlinear behavior and a full-scale experimental reinforced concrete benchmark show the potential and applicability of the method proposed for the integrity assessment of civil structures.

KEYWORDS

clustering, damage identification, nonlinear normal mode, nonlinear structure, time-frequency representation, time-varying feature

1 | INTRODUCTION

In nature, the dynamic behavior of structures generally follows nonlinear laws.¹ In civil engineering, there are several sources of nonlinearity, mostly related to material behavior (i.e., constitutive laws), geometry (whenever the magnitude of the displacements affects the structural response), and boundary conditions.^{2,3} Several studies also show how nonlinearities usually increase in damaged structures, for which cracks and loosening of connections may occur.^{3,4}

In the context of vibration-based structural health monitoring (SHM), “linearity” is a necessary assumption for using classical modal analysis methods. Thus, nonlinearities are usually overlooked during the application of operational modal analysis, relating to the fact that ambient vibration is modest, and the effects of nonlinearities are noticeable only under high-energy excitation.⁵

One of the latest trends in the field of SHM is known as seismic structural health monitoring (S²HM),⁶ for which recordings obtained during seismic events are used for dynamic identification and model updating. This approach allows

This is an open access article under the terms of the [Creative Commons Attribution](https://creativecommons.org/licenses/by/4.0/) License, which permits use, distribution and reproduction in any medium, provided the original work is properly cited.

© 2021 The Authors. *Earthquake Engineering & Structural Dynamics* published by John Wiley & Sons Ltd.

the assessment of damage in the aftermath of an earthquake, avoiding the effects of temperature or variable environmental conditions which may alter the parameters identified through long-term procedures.⁷

Improvements in the field of microelectromechanical systems and wireless smart sensor networks, which lead to increased energy efficiency and to the possibility of collecting high-fidelity data, have recently enabled the development of event-triggered sensing systems.⁸ These systems are designed to collect data (usually consisting of acceleration recordings) only when a certain amplitude threshold is exceeded. The transmission of a short dataset to the monitoring station is far more efficient than a transmission carried out during a continuous monitoring procedure. Furthermore, recordings obtained during strong events usually have a high signal-to-noise ratio, which allows the structural characterization even with short data series. However, in the case of strong events, many systems, such as reinforced concrete (RC) structures, may manifest strong nonlinearities, which can no longer be even assimilated to a linear behavior. In fact, according to current codes, civil structures are designed with certain ductility requirements to take advantage of the excursion in the nonlinear field during earthquakes.³

Since the use of nonlinear structural elements is increasingly growing in engineering applications, several studies have recently been conducted on modeling and identification of nonlinear structures.⁹

The basic principles usually assumed for modal identification of linear systems (such as the superposition principle) may be no longer usable in the presence of nonlinearities. In this case, modal responses cannot be studied separating space and time information and the traditional concept of “vibration modes” is no longer applicable. Rosenberg¹⁰ first extended this concept by defining a nonlinear normal mode (NNM) of an undamped system as a synchronous (vibration in-unison) periodic oscillation where all material points of the system reach their extreme values and pass through zero simultaneously. This definition is also usable in the case of weakly damped systems and enables the description of nonlinear structures employing a (nonlinear) modal curve in the configuration space.³

Several identification algorithms for nonlinear systems operating in time,^{11,12} frequency,⁴ and time-frequency¹³ domain have been proposed in the last decades. Also, model-based^{14,15} and black-box¹⁶ techniques are taking a step into SHM applications, based upon finite element model updating and artificial neural networks.

In the time domain, recursive approaches for estimating time-varying structural features have been largely investigated. Loh and Lin identified time-varying natural frequencies and damping ratios employing single-input and single-output pairs consisting of the ground excitation and the structural response, respectively.¹⁷ More recently, Bhowmik et al. used the recursive canonical correlation analysis to implement a reference-free damage identification method for online applications.¹⁸ Recursive approaches, however, generally need a convergence interval, which makes them not suitable for short-term event-triggered applications. The Hilbert–Huang transform (HHT),¹⁹ that is, the Hilbert transform (HT) applied to the intrinsic mode functions (IMFs) obtained through the empirical mode decomposition, is currently one of the most largely used time-domain techniques for the instantaneous description of structural resonant frequencies and modal amplitudes.^{11,12,20} However, this method is affected by known mode-mixing problems, for which noise-assisted and multivariate improvements have been proposed.^{21,22}

The instantaneous description of dynamic features is also obtainable by applying transforms that enable time-frequency representations (TFRs) of the signal. The wavelet transform has been widely employed in research, including studies concerning nonlinear dynamic systems.¹³ The S-transform has recently been exploited by Ditommaso et al.²³ through an adaptive filter bank to extract decoupled energy-dependent modal responses from multicomponent signals, providing an estimate of the instantaneous dynamic parameters. In particular, Ditommaso et al. analyzed the dynamic behavior of structures under seismic excitation, considering the mode shape related to the minimum frequency recorded during the maximum excursion in the plastic field as a damage-sensitive feature (DSF). Other developments of this method gave rise to reliable damage localization algorithms.²⁴ Recently, Quqa et al.²⁵ presented a novel TFR usable for the near-real-time visualization and extraction of instantaneous modal parameters of dynamic systems. The modal assurance distribution (MAD) presented in the mentioned paper highlights valuable information for the extraction of decoupled modal responses for linear time-varying systems.

The present work has three main goals: (1) verify the applicability of MAD to nonlinear dynamic responses, considering the Rosenberg definition of NNM; (2) propose an extended decomposition algorithm suitable for short-term applications (e.g., using recordings collected by event-triggered systems) to extract time-domain representations of the NNMs; (3) use the identified parameters for damage identification in output-only conditions. The proposed technique is based on the multivariate analysis of structural responses, that is, all the collected vibrational recordings are processed together. This aspect involves important advantages over most of the identification methods based on the analysis of one-dimensional signals, where different structural features could be identified at each instrumented location.

The analysis of two case studies, a nonlinear numerical model and an experimental full-scale RC benchmark, both subjected to seismic motions, proves the potential of the method proposed. In particular, the identified modal parameters

show a detailed description of the structural behavior during the nonlinear excursion due to the strong motion. Moreover, a flexibility-based approach is used to evaluate instantaneous damage indices, which can be exploited for the assessment of the structural integrity in the aftermath of a seismic event.

2 | MODAL ASSURANCE DISTRIBUTION

The wavelet packet transform (WPT) is a particular case of discrete wavelet transform that can be employed to represent a signal into the time-scale domain by filtering the original sequence through high-pass and low-pass wavelet filters (and downsampling the outcomes) following the Mallat recursive algorithm,²⁶ or employing equivalent filters obtained through convolution (and upsampling) of the wavelet filters following a specific order.²⁷ The outcomes of this filtering process are the wavelet components (or signal subbands). The two-dimensional representation of a signal into the time-scale domain, generated using the squares of the obtained wavelet components, is called scalogram and can be converted into a TFR using the relation that exists between scales and frequencies.²⁷ The scalogram is generally used as a representation of the energy distribution of the analyzed signal into the time-scale plane and is employed to visualize the presence of resonant signal components, which generate high-valued areas. Such resonant components are commonly interpreted as the modal components (or modal responses) of the analyzed signal in SHM applications.

The wavelet components obtained using WPT contain frequency-band-limited information of the original signal over time. The width f_w of the frequency band described by each component (and then the frequency resolution of the scalogram) depends on the level of the transform (n) and the sampling frequency of the original signal (F_s), resulting in $f_w = F_s / 2^{n+1}$. Moreover, selecting a transform level n , the original signal is represented by 2^n wavelet components, each corresponding to a specific frequency band (referred to as “frequency subband”), which are evaluated through WPT.

Operating deflection shapes (ODSs) have been traditionally defined as the deflection of a structure at a particular frequency of excitation.⁵ Information related to both the forcing input and the resonant structural components is generally fused into ODSs, while mode shapes are inherent properties of the structure. However, it can be assumed that near to the resonance peak of the frequency response spectrum, ODSs are dominated by structural modes. In modal identification, ODSs evaluated at resonant frequencies are, therefore, assumed as fair approximations of the mode shapes. Similar to traditional identification methods where amplitudes of the Fourier spectra of a set of structural responses are assumed to form ODSs, the values of the wavelet components related to a given time instant and a given frequency subband of each recording channel can be interpreted as the elements of an instantaneous ODS. The vector generated collecting these elements represents, indeed, the amplitude of the signal for a specific (narrow) frequency range at all the instrumented locations. Depending on f_w , a resonant component in the scalogram may be described by multiple wavelet components. In other words, a modal response may have a frequency range larger than f_w , depending on damping. Thus, performing the WPT of structural responses, each resonant component is likely to be represented by a set of wavelet components with consecutive subband index (i.e., neighboring components on the frequency axis).

The MAD is a TFR based on the idea that the wavelet components obtained through WPT of a set of structural responses will form ODSs, which are instantaneously similar to each other if they refer to the same resonant component. In this case, the ODSs will be an approximation of the mode shapes of the structure. Moreover, due to the orthogonality property of vibration modes, the ODSs of two different modal responses will likely to be orthogonal. The MAD is thus a map in the time-frequency plane that indicates the “similarity” of neighboring ODSs obtained by applying the WPT to the channels of a multivariate signal consisting of structural responses. In the original formulation,²⁵ the MAD is obtained for long-term applications to linear time-varying structures. In this paper, the concept behind this technique is exploited to obtain a novel formulation of the MAD applicable to the response of nonlinear systems even for short-term applications, such as the analysis of the structural behavior during earthquakes. The instantaneous identification of resonant components in this situation enables the extraction of a time-domain description of NNMs during the structural nonlinear excursion, which may provide valuable information for the evaluation of the structural integrity in the aftermath of a seismic event. However, due to the significant differences that exist between the long-term linear case²⁵ and the short-term nonlinear situation addressed in this study, a novel identification algorithm is proposed hereinafter.

In this section, first, the basic theory of MAD is reported and extended for applicability to nonlinear problems. A novel decomposition algorithm is then proposed, explaining how decoupled normal modes can be extracted from a multivariate signal and analyzed to retrieve instantaneous dynamic parameters usable for damage identification during seismic strong motions.

2.1 | Original formulation

The MAD is a TFR of multivariate and multicomponent signals used to highlight the presence of different modal responses based on the analysis of signal subbands obtained through a preliminary time-frequency decomposition. In the original formulation,²⁵ the decomposition of each channel of the multivariate signal is performed through the WPT, which enables the extraction of nonredundant wavelet coefficients representative of localized (in frequency and time) dynamic features. For each time instant t and frequency subband k (with $k = 1, \dots, 2^n$, and n denoting the transform level), an instantaneous ODS $\varphi_k[t]$ can be evaluated considering the corresponding wavelet coefficients obtained from each data channel. The normalized elements of the column vector $\varphi_k[t]$ over a reference location r can thus be evaluated as:

$$\varphi_{i,k}[t] = \frac{d_{i,k}^{(n)}[t]}{d_{r,k}^{(n)}[t]}, \quad (1)$$

with $d_{i,k}^{(n)}[t]$ denoting the t -th sample of the wavelet coefficients at the transformation level n related to the subband k obtained by decomposing the signal collected at the location i . The similarity between the ODSs obtained for neighboring subbands k and $k+1$ at a given time instant is then evaluated through the modal assurance criterion, from which the method takes its name. The elements of MAD are, therefore, defined as:

$$m_k[t] = \frac{|\varphi_k^T[t] \varphi_{k+1}[t]|^2}{(\varphi_k^T[t] \varphi_k[t]) (\varphi_{k+1}^T[t] \varphi_{k+1}[t])}. \quad (2)$$

Assuming that each channel of the multivariate signal consists of the structural response (given by modal superposition) plus instrumentation noise, and considering a high transformation order, such that each resonant component in the analyzed signal is represented by more than one wavelet component, persistent high values in the MAD (i.e., close to 1) will appear in the time-frequency areas where modal responses are present. On the other hand, random similarities between noise-generated ODSs will give rise to beta-distributed noise with values in the range between 0 and 1. In order to improve the readability of the MAD, two approaches were also proposed.²⁵ The former consists of averaging the MAD estimates using a forgetting factor which gives exponentially less weight to older samples in the time domain, while the latter involves a noise-assisted criterion that consists of evaluating the average MAD $\tilde{m}_k[t]$ obtained by an ensemble of L MADs $m_k^{(\lambda)}$ computed on the original signal plus different Gaussian white noise components:

$$\tilde{m}_k[t] = \frac{1}{L} \sum_{\lambda=1}^L m_k^{(\lambda)}[t]. \quad (3)$$

The original formulation of MAD was only used to analyze linear time-varying systems, with the assumption of piecewise-constant dynamic parameters. Indeed, the WPT is characterized by shift-variance that makes it unsuitable for the evaluation of instantaneous ODSs using short recordings collected during seismic events. Moreover, a forgetting factor cannot be considered to improve the readability of the distribution due to the loss of accurate time information.

2.2 | Modal assurance distribution for S²HM

A particular dynamic feature of nonlinear systems consists of the frequency-energy dependency of their oscillations that involves variations in the frequency response functions depending on the level of excitation.¹ Thus, frequencies and amplitudes of NNMs are typically time-varying and energy-dependent. Considering a structure with nonlinear displacement-dependent stiffness, excited by a generic forcing function, assume the discrete-time acceleration response collected by an

accelerometer deployed at the i -th material point as the combination of p dominant resonant components $\ddot{q}_j[t]$:

$$\ddot{x}_i [t] = \sum_{j=1}^p \phi_{i,j} [t] \ddot{q}_j [t] + v_i [t], \quad (4)$$

where $\phi_{i,j}[t]$ is the i -th element of a time-varying and energy-dependent j -th mode shape, $q_j[t]$ is a monocomponent function of time with a narrow frequency band (generally, depending on the damping) centered around the time-varying and energy-dependent damped frequency $\omega_{d,j}[t]$, $\ddot{q}_j[t]$ is its double time derivative, and $v_i[t]$ is the recording noise, modeled here as a Gaussian white noise component. In general, p can be considered as the number of dominant resonant components in the structural response that exceed the noise threshold given by the $v_i[t]$ term. Each term of the summation in Equation (4) is called here nonlinear modal response (NMR) and represents the time-domain description of a single NNM during the application of a given excitation.

In general, assuming $\phi_{i,j}[t]$ as a nonzero-mean function, its Fourier transform $\Phi_{i,j}[\omega]$ evaluated in $\omega = 0$ is $\Phi_{i,j}[0] \neq 0$. Moreover, other peaks in the spectrum of $\Phi_{i,j}[\omega]$ appear centered at frequencies $\omega_{\bar{k}}$, which depend on the nature of nonlinearity and the instantaneous frequencies of the system (which, in turn, depend on the energy of excitation). Also, assume that $\Phi_{i,j}[0] \gg \Phi_{i,j}[\omega_{\bar{k}}]$, that is, the fluctuations in time of the elements of instantaneous mode shapes around their mean values have modest amplitude compared to their mean values. This assumption should be verified by observing the final results of the identification procedure. However, in general, the nonlinear excursion slightly affects the mode shapes. Moreover, the frequency spectrum of the noise component $V_i[\omega]$ assumes constant values that can be considered as negligible compared to the amplitude of the NMRs if high-performance accelerometers are employed (i.e., having high resolution and sensitivity, and low noise floor, such as the specific instrumentation typically used for SHM applications⁵).

For a given mode \hat{j} , according to the convolution theorem, the product between $\phi_{i,\hat{j}}$ and $\ddot{q}_{\hat{j}}$ in the time domain is equivalent to a convolution between their Fourier spectra in the frequency domain (indicated as $\Phi_{i,\hat{j}}[\omega]$ and $Q_{\hat{j}}[\omega]$, respectively). Through the assumptions made above, considering a time-windowed slice of the structural response such that the frequency spectrum has clear peaks at the instantaneous natural frequency values, the following relation is admissible if modes are well distanced:

$$\left(\Phi_{i,\hat{j}} * Q_{\hat{j}} \right) [\omega_{\hat{j}}] \approx \sum_{j=1}^p \left(\Phi_{i,j} * Q_j \right) [\omega_{\hat{j}}], \quad (5)$$

with $*$ denoting the convolution operator and $\omega_{\hat{j}}$ the frequency value, where $(\Phi_{i,\hat{j}} * Q_{\hat{j}})[\omega]$ reaches its maximum. Thus, considering a narrow bandpass filter centered in $\omega_{\hat{j}}$ with impulse response described by $b_{\hat{j}}[t]$,

$$\frac{(b_{\hat{j}} * \ddot{x}_i)[t]}{(b_{\hat{j}} * \ddot{x}_r)[t]} \approx \frac{\phi_{i,\hat{j}}[t]}{\phi_{r,\hat{j}}[t]}, \quad (6)$$

where r indicates a reference location. Assuming the Rosenberg definition of NNM, the ratio on the right-hand side of Equation (6) represents a point in the two-dimensional projection of the configuration space onto the directions of i and r . Indeed, different points in the configuration space can be evaluated considering specific time instants of the narrow frequency subband of the multicomponent signal that instantaneously isolates a single NMR.

Considering a generic frequency value ω_k , Equation (5) is no more valid for frequencies far from $\omega_{\hat{j}}$. Moreover, $V_i[\omega_k]$ may be non-negligible compared to $\sum_{j=1}^p (\Phi_{i,j} * Q_j)[\omega_k]$. In particular, considering a narrow bandpass filter with central frequency $\omega_k \neq \omega_{\bar{k}}$, the noise component is likely to prevail, leading to $(b_k * \ddot{x}_i)[t] \approx (b_k * v_i)[t]$. On the other hand, in $\omega_k = \omega_{\bar{k}}$, the frequency component generated by the variability of $\phi_{i,j}[t]$ may lead to spurious peaks in the frequency spectrum of $\ddot{x}_i[t]$. However, considering the assumptions made, such peaks have modest amplitudes, proportional to the fluctuations of the elements of mode shapes.

In general, the i -th element of the ODS associated with the k -th subband can be computed as:

$$\varphi_{i,k} [t] = \gamma_k^{(t)} \frac{(b_k * \ddot{x}_i)[t]}{(b_k * \ddot{x}_r)[t]}. \quad (7)$$

However, calculating $\varphi_{i,k}[t]$ for different values of $k = 1, \dots, 2^n$ for the evaluation of the MAD, the following three different situations can occur:

1. Using b_k with central frequency $\omega_k = \omega_j$ (i.e., coinciding with an instantaneous natural frequency of the system), $\varphi_{i,k}[t]$ represents an element of the j -th instantaneous mode shape and Equation (7) becomes equivalent to Equation (6).
2. Using b_k with central frequency $\omega_k = \omega_{\bar{k}}$ (i.e., coinciding with a signal component generated by the fluctuations of mode shapes), $\varphi_{i,k}[t]$ depends on the nature of nonlinearity.
3. Using b_k with central frequency ω_k different from the previous conditions, $\varphi_{i,k}[t]$ varies over time without reflecting the structural behavior (i.e., the ratio between filtered noise components).

The MAD can thus be computed even in the case of nonlinear structural responses using the ODS obtained as shown in Equation (7). In this case, however, the spurious similarity of neighboring ODSs generated by time-varying modal amplitudes must be taken into account. In particular, if the inequality $\Phi_{i,j}[0] \gg \Phi_{i,j}[\omega_{\bar{k}}]$ is not verified, the readability of the MAD may be affected, making the identification of NNMs challenging.

Differently from other TFRs that represent the energy of the signal in a time-scale or time-frequency plane, the MAD only relies on the “similarity” between ODSs. In other words, the magnitude of the wavelet components and, therefore, the level of excitation in a given frequency range, has not a fundamental role in MAD formation, which only depend on the ratios between wavelet components generated at different locations. Thus, the only requirement for the application of the proposed method is that the level of excitation in all the considered frequency range generates a structural response, which exceeds the noise floor of the instrumentation. This requirement is generally satisfied in all SHM applications and is much less demanding than the typical assumption involving white noise excitation.

In this paper, a filter bank formed of the bandpass filters $b_k = d_k * r_k$ is considered, with d_k and r_k denoting the k -th equivalent decomposition and reconstruction filters associated with an n -th level stationary wavelet packet transform (SWPT). The size and performance of these filters were investigated in a previous work,²⁸ showing their applicability to near-real-time identification procedures.

2.3 | Instantaneous structural identification

Based on the idea that signal subbands forming similar instantaneous ODSs are likely to belong to the same modal component, a new algorithm for the decomposition of nonlinear structural response into decoupled NMRs is proposed in this section. In this context, the MAD is used as the starting point of the algorithm, necessary to select the wavelet components corresponding to physical modes over those describing noise. As discussed before, the use of a forgetting factor is not indicated to improve the readability of the MAD when dealing with short and strongly nonstationary recordings. Although the noise-assisted approach may still be pursued, the final distribution may be noisy and not suitable for the application of image processing techniques, such as the watershed transform²⁵ for the extraction of decoupled NMRs. Moreover, due to the strong nonstationarity of seismic events, clear ridges in the MAD may not be visible and disconnected areas may belong to the same NMR. For these reasons, a clustering procedure is applied to partition the instantaneous ODSs into sets referring to separate modes. Upon reconstructing the signal of each identified cluster, the instantaneous parameters of decoupled structural responses can be exploited for damage identification. The procedure proposed in this work for the extraction of decoupled modal responses is illustrated in Figure 1 and explained in detail below.

First, the instantaneous ODSs obtained in Equation (7) from the filtered components of the multivariate signal are used to evaluate an MAD, as shown in Equation (2). A decomposition matrix \mathbf{M} , having the same size of the MAD, is then generated using the following rule:

$$\mu_k [t] = \begin{cases} 1 & \text{if } m_k [t] \geq \eta \\ 0 & \text{if } m_k [t] < \eta \end{cases}, \quad (8)$$

where $\mu_k [t]$ is a generic element of \mathbf{M} (k denotes the row index and t is the column index) and η is a user-defined threshold. The optimal value of η can be determined by analyzing the residuals of the decomposition algorithm.²⁵ However, $\eta = 0.5$ can be generally adopted and a lower value may be considered depending on the number of instrumented locations if the noise-assisted procedure is carried out.

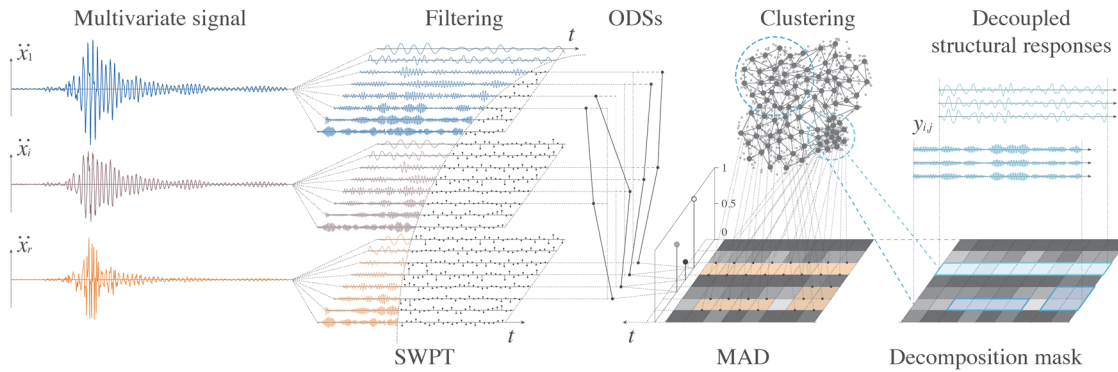


FIGURE 1 Workflow of the procedure proposed

The \mathbf{M} matrix represents a “mask” of 1 and 0 values that selects high-valued areas in the MAD. Morphological operations, such as erosion, can be applied to \mathbf{M} if a high transformation level is selected for signal decomposition since filter overlaps may origin spurious ODS similarities.²⁸ In a morphological operation, each element $\mu_k[t]$ is interpreted as a pixel in the time-frequency distribution and is adjusted based on the value of neighboring pixels.²⁹ Erosion, in particular, replaces each value with the local minimum of its neighborhood and can be used to remove spurious elements. Considering the matrix $\tilde{\mathbf{M}}$, obtained using morphological operations on \mathbf{M} , the set S of ODSs representing physical modes is generated by selecting, among the $\varphi_{i,k}[t]$ identified using Equation (7), only the ODSs similar to each other in the neighboring subbands, that is, generating high MAD values and, hence, 1 values in the $\tilde{\mathbf{M}}$ matrix. This selection procedure can, therefore, be written as:

$$\varphi_k[t], \varphi_{k+1}[t] \in S \Leftrightarrow \tilde{\mu}_k[t] = 1, \quad (9)$$

where $\varphi_k[t] = [\varphi_{1,k}[t], \dots, \varphi_{r,k}[t]]^T$ and $\tilde{\mu}_k[t]$ is a generic element of $\tilde{\mathbf{M}}$.

The k-means algorithm³⁰ is thus applied to partition the set of selected instantaneous ODSs into different clusters referring to separate modes. However, the number of clusters is a parameter required to initialize the k-means algorithm and, especially when dealing with high-dimensional data, its determination is not straightforward. For this reason, in this study, a self-organizing map (SOM)³¹ is employed to help the user in the selection of the optimal number of clusters.

SOM is a type of unsupervised neural network that generates a low-dimensional (generally two-dimensional) representation of the input space (the dimension of which is equal to the number r of channels that form the multivariate signal) approximating the data distribution through a user-defined number of neurons.³¹ These neurons, upon training the neural network, can be represented on a regular grid with hexagonal or rectangular mesh to visualize the obtained low-dimensional approximation of the input data. This process is possible since the trained map preserves the topological properties of the input space. Thus, the visualization of the U-matrix, that is, the map of Euclidean distances between the weight vectors of an SOM (that are the coordinates of each neuron in the input space) may be useful for the selection of the number of clusters. Upon training the SOM, the input data (that in this application consists of the r -dimensional ODSs) can, indeed, be represented on a plane, where the number of clusters can be visually (or automatically, using suitable algorithms) inferred.

It is worthy to note that the step involving SOMs is not strictly necessary for the aim of this procedure; however, it may facilitate the selection of the number of clusters. Moreover, due to the variability over time of ODSs during the nonlinear excursion, nonconvex clusters may be generated in the original ODS space. However, the approximation generated by the SOM generally mitigates this phenomenon. Therefore, applying the k-means algorithm to the weights of the neurons of the trained SOM may improve the performance of the decomposition technique. In this case, however, a further step is required to generate the final sets of ODSs associated with different modes. The clusters of weight vectors should, indeed, be converted into sets of original ODSs by selecting the elements of the original space classified by each neuron in the obtained clusters.

In this work, the k-means algorithm is applied to the weight vectors obtained upon training the SOM using the input ODSs. After using the k-means method, in order to retrieve the clusters in the input space, the ODSs are associated with the cluster C_j of the neuron which classifies them. Once the clustering process is completed, a reconstruction mask \mathbf{R}_j is

built for each cluster C_j , selecting the elements of the filtered signals previously used to generate the clustered ODSs. The elements $\rho_{j,k}[t]$ of \mathbf{R}_j can thus be built as:

$$\rho_{j,k}[t] = \begin{cases} 1 & \text{if } \varphi_k[t] \in C_j \\ 0 & \text{otherwise} \end{cases}. \quad (10)$$

Due to the perfect reconstruction property of the selected filter bank, the decoupled j -th NMR $y_{i,j}[t]$ associated with the location i can be directly retrieved by summing the filtered components associated with the same cluster for each time sample:

$$y_{i,j}[t] = \sum_{k=1}^{2^n} \rho_{j,k}[t] (b_k * \ddot{x}_i)[t]. \quad (11)$$

It is worthy to note that the process described above can be seen as the construction of a signal-adaptive filter bank with band-variable filters capable of extracting decoupled modal responses through cutoff frequencies selected based on the clustering process. This process can be, therefore, intended as an adaptive generalization of the clustered filter bank procedure proposed in a previous work²⁸ for applications with decentralized smart sensor networks.

Upon reconstruction, each monocomponent NMR can be processed through the HT to evaluate its instantaneous frequency, which is interpreted here as one of the time-varying natural frequencies of the nonlinear structure. Moreover, the j -th time-varying mode shape $\phi_j[t]$ can be evaluated considering the vector $\mathbf{y}_j[t]$ of NMRs normalized over a reference value $y_{r,j}[t]$:

$$\phi_j[t] = \frac{\mathbf{y}_j[t]}{y_{r,j}[t]}. \quad (12)$$

3 | APPLICATIONS

In this section, the MAD is evaluated for two nonlinear case studies. The NMRs are extracted through the presented procedure and instantaneous modal parameters are identified, enabling the application of a flexibility-based method for damage identification. It is shown how the dynamic behavior of the structure during the maximum excursion in the nonlinear field can be related to the structural damage, manifesting effects which cannot be identified using low-amplitude ambient vibration. In particular, the localized increase in curvature in flexural-type structures or anomalous interstory displacements in shear-type frames can be detected using the instantaneous flexibility matrix built from the modal parameters identified during the seismic event. If these effects vanish or are attenuated in the short term, they may indicate the presence of breathing cracks.

3.1 | Case study 1: numerical simulation

The first case study considered in this work is a two-dimensional, four degrees of freedom (DOFs), shear-type frame with masses equal to $m = 8 \cdot 10^4$ kg, damping coefficients equal to $c = 5 \cdot 10^5$ Ns/m, and stiffness consisting of a linear part equal to $k_l = 2 \cdot 10^8$ N/m plus a nonlinear part, which is a function of the displacement, modeled to simulate a softening behavior, typical of RC frame structures. In particular, the equation of motion of the i -th level of the system can be written as:

$$m\ddot{x}_i + c \sum_{j=1}^r p_{i,j} \dot{x}_j + \sum_{j=1}^r p_{i,j} (k_l x_j + k_3 x_j^3 + k_5 x_j^5) = -m\ddot{s}, \quad (13)$$

where x_j is the relative displacement of the j -th DOF with respect to the ground, $k_3 = -3 \cdot 10^{11}$ N/m³ and $k_5 = 1.8 \cdot 10^{14}$ N/m⁵ are the nonlinear stiffness coefficients, \ddot{s} is the acceleration of the seismic motion applied at the base of the structure, and $p_{i,j}$ are the elements of a tridiagonal matrix with $p_{i,i} = 2$ on the main diagonal, except for $p_{r,r} = 1$ (i.e.,

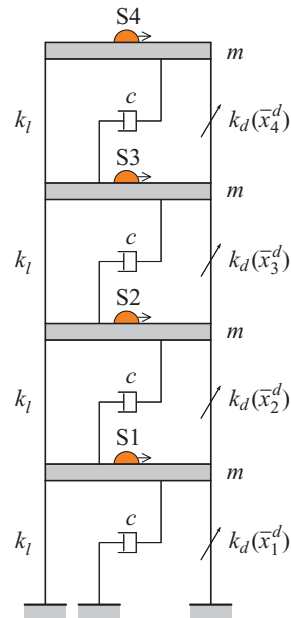


FIGURE 2 Schematic of the numerical model

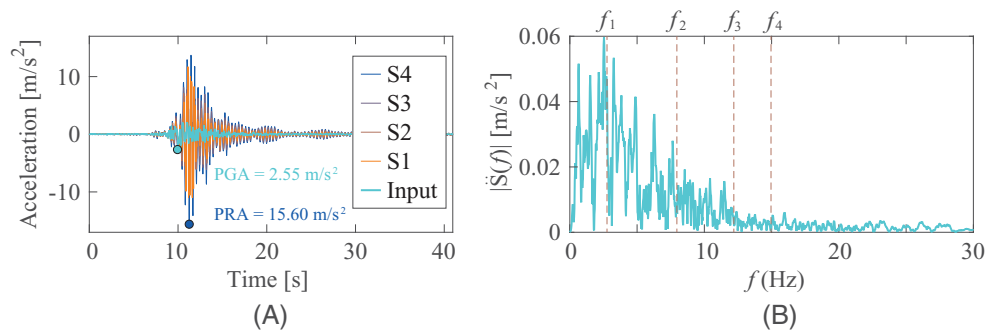


FIGURE 3 Structural responses of the numerical model (A) and frequency spectrum of the seismic ground acceleration (B)

at the top level of the frame), and $p_{i,j} = -1$ in the other nonzero elements. The nonlinear stiffness coefficients were selected to simulate strong softening nonlinear effects in the displacement range of the structural response, keeping the overall instantaneous stiffness always positive. In linear conditions, that is, only considering the linear stiffness k_l , the natural frequencies of the numerical benchmark are 2.76, 7.96, 12.19, and 14.96 Hz.

At each level, a simulated uniaxial sensing device was considered, recording the absolute acceleration of the system in the direction of the seismic motion. A scheme of the case study with the deployment of simulated sensors (indicated as S#) is reported in Figure 2. In this test, the seismic motion recorded by the station located in Mirandola (Italy) during the Emilia earthquake of May 20th, 2012 was used. The acceleration time histories collected by each simulated sensor with a sampling frequency of 50 Hz, together with the input excitation, are reported in Figure 3A. Here, PGA indicates the peak ground acceleration, while PRA indicates the peak response acceleration at the top level. The total duration of the recording is 40.96 s. In order to simulate the instrumentation noise, a white Gaussian noise component with a standard deviation of 0.02 m/s^2 (i.e., the 1.11% of the standard deviation of the response collected at the top of the building, or the 0.13% of the peak response collected at the same point) was included in the analyzed response. The Fourier spectrum of the input excitation is reported in Figure 3B, where the natural frequencies f_j of the benchmark are also indicated. In this figure, it is possible to notice that the first mode is the most stimulated by the Emilia earthquake, while the others are less excited.

Between time instants 10.70 s and 11.60 s, a uniform decrease (following a linear function) of k_l in time was induced at the base level to simulate progressive damage, passing from the “undamaged” State 1 to a “damaged” State 2 with a final linear stiffness of $1.8 \cdot 10^8 \text{ N/m}$. A representation of the force-displacement and stiffness-displacement diagrams obtained

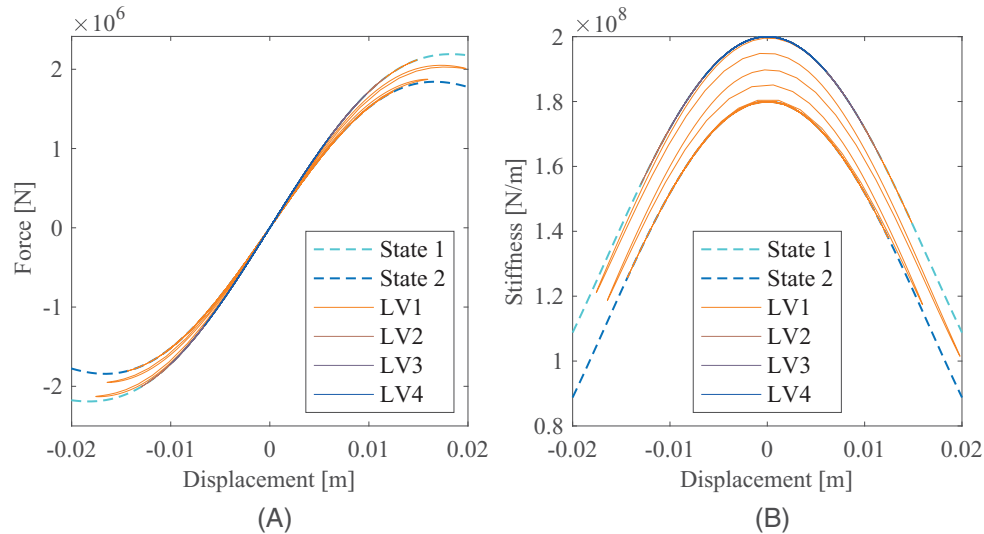


FIGURE 4 Force-displacement (A) and stiffness-displacement (B) diagrams of each level (LV)

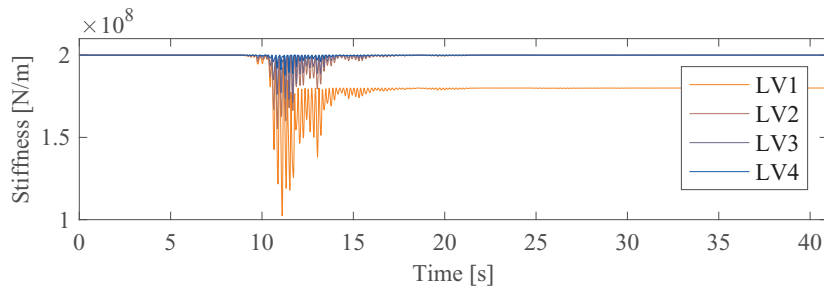


FIGURE 5 Instantaneous stiffness of each level

during the dynamic tests is reported in Figure 4 for each level. Moreover, the instantaneous stiffness of each level in time is represented in Figure 5. From this last graph, it is possible to notice that the excursion in the nonlinear field leads to much lower instantaneous stiffness values than the residual stiffness of the damaged condition, for all the levels.

Using the multivariate signal consisting of the four acceleration channels collected by sensors S1, S2, S3, and S4, an MAD was computed following the noise-assisted approach. In particular, an ensemble of 100 different white Gaussian noise sets with a standard deviation of 0.05 m/s^2 were added to the collected structural responses to obtain the average distribution reported in Figure 6. Here, MAD values are represented in a time-component plane where the component axis represents the k index used in Equation (7), indicating the frequency bands. In this figure, orange areas indicate $m_k[t]$ values close to 1, while blue areas indicate values close to 0. A mask matrix was then built, as described in Equation (8), to select the ODSs that generated MAD values over a threshold $\eta = 0.5$.

In order to apply the k-means algorithm, the number of clusters was determined by analyzing the U-matrix of an SOM trained with the selected set of ODSs that generated MAD values over the selected threshold. The map is sized considering that the SOM is a quantizing method and, to have a satisfactory resolution to visualize the data distribution, at least 50 items (on average) should be classified by each node, otherwise, the resolution of the outcome will be limited by the sparsity of data. Moreover, the array of neurons should have horizontal and vertical dimensions complying with the largest principal

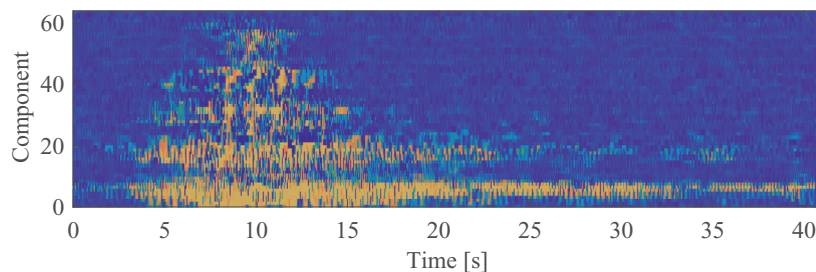


FIGURE 6 Modal assurance distribution

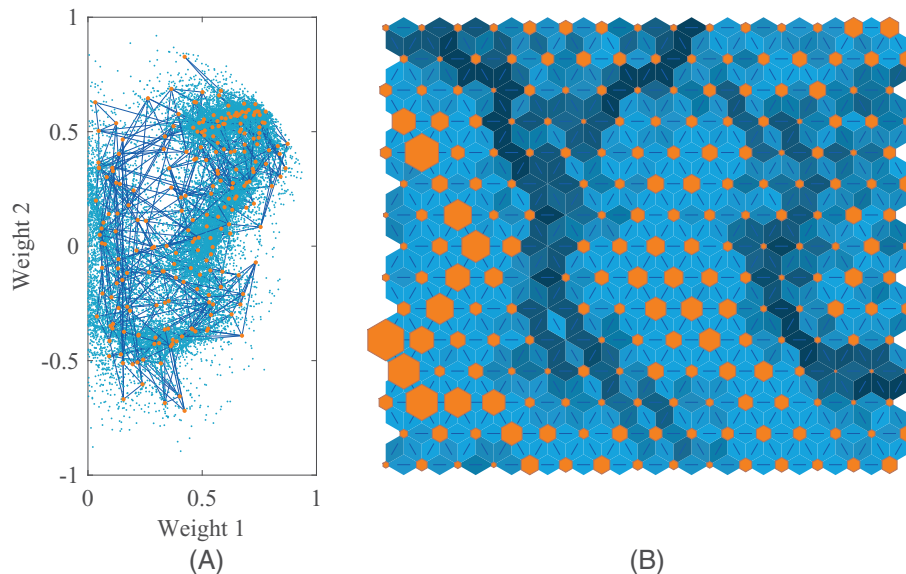


FIGURE 7 Self-organizing map (A) and corresponding U-matrix (B)

components of the input data.³² Therefore, in this study, the number of neurons is selected as a number close to $N/100$, with N denoting the number of observations (i.e., the 26,091 selected ODSs), forming a square array. Indeed, since the input vectors are normalized ODSs, that is, vectors lying on the surface of an r -dimensional hypersphere, the variance explained by their first two principal components is likely to be the same. In particular, a 15×15 map with a hexagonal grid consisting of 225 neurons was employed.

The training process was performed over 200 epochs, in which all the selected ODSs are used to update the weights of neurons in batch mode (i.e., at the end of each epoch). In Figure 7, two representations of the trained SOM are reported. Figure 7A shows a two-dimensional projection of the neurons (orange dots) and the connections of the SOM (blue lines) onto the first two weights, that is, the DOFs of the structure corresponding to levels 1 and 2. Here, the light blue points are the vectors of the input space. On the other hand, Figure 7B shows the U-matrix of the SOM, that is, a low-dimensional representation of the selected ODSs. In this figure, the neurons are depicted as orange hexagons, while the color of their connections depends on their Euclidean distance. In particular, light blue connections denote close neurons, while dark blue connections denote larger distances. Moreover, the size of the hexagons of Figure 7B is proportional to the number of ODSs classified by each cluster. From a visual analysis of the U-matrix, it is easier to identify a reasonable number of clusters, that is, dense areas in the low-dimensional distribution. These areas are light blue regions populated by large orange hexagons, delimited by dark blue boundaries. In this study, four clusters can be clearly identified, the first in the left-lower region, the second from the central part to the right-lower corner, the third in the right-upper region, and the fourth in the left-upper part. Although in this work a manual selection of the number of clusters is performed, image processing techniques can be applied to the U-matrix to automatically identify the most likely number of clusters.³³

The k-means algorithm was then applied to the weight vectors of the neurons, partitioning the set of selected ODSs into four clusters. An illustration of the clustered ODSs is reported in Figure 8A, where the instantaneous wavelet components associated with the selected ODSs are represented as points in the time-component plane, with a color depending on the belonging cluster. In Figure 8B, the ODSs associated with each point of Figure 8A are illustrated in the space domain, along with the height of the structure. Moreover, the average trend of each cluster is indicated as an orange dashed line. It is possible to observe how the shapes belonging to the same cluster are similar between each other and the average curves may be interpreted as an estimate of the mode shapes of the structure. However, in this phase, it is not possible to distinguish between ODSs before and after the seismic event, that is, possibly referring to an “undamaged” and a “damaged” condition since, in this case, the differences are minimal compared to the variability of the ODSs in a given cluster. More sophisticated clustering methods not requiring the knowledge of the number of clusters may also be applied, such as the density-based spatial clustering of applications with noise,³⁴ which is, however, very sensitive to the distance thresholds, that is another parameter required in the mentioned procedure. On the other hand, the SOM-based criterion is not very sensitive to the number of neurons forming the map, which is the only parameter needed for the realization of the U-matrix.

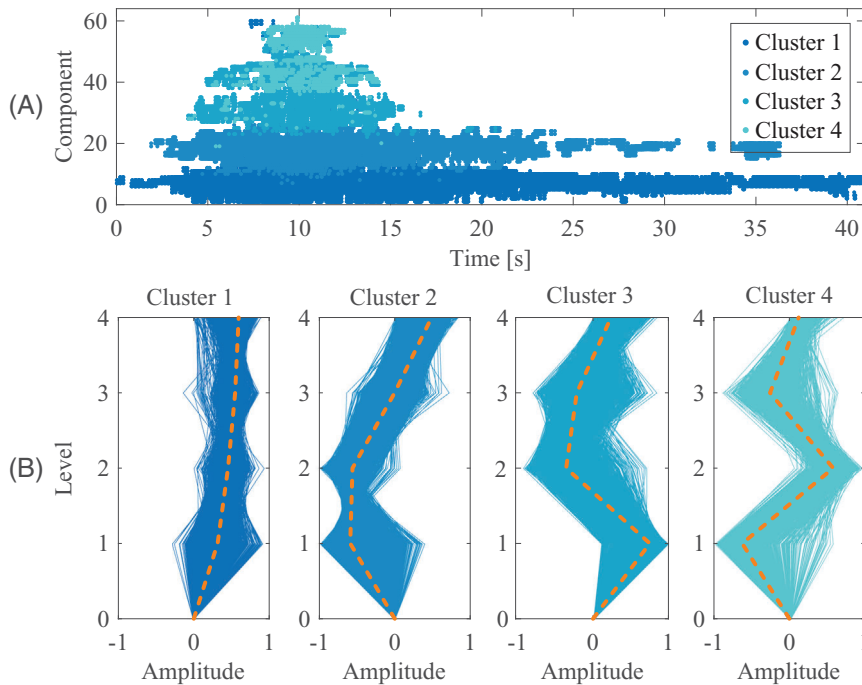


FIGURE 8 Result of the clustering procedure

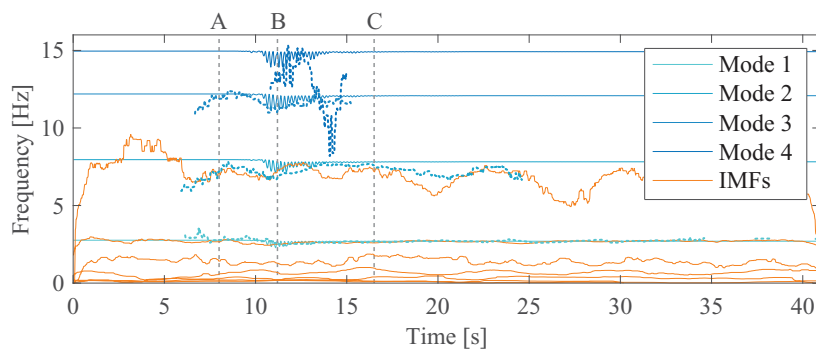


FIGURE 9 Instantaneous natural frequencies (theoretical in solid lines and identified in dashed lines) and results of the Hilbert–Huang transform

The NMR of each identified node was then reconstructed by summing the wavelet components used to obtain the ODSs referring to a given cluster (i.e., to a single modal component). The instantaneous resonant frequencies were thus identified using the HT. In this study, the HHT is also considered to have a comparison with one of the most used techniques for the instantaneous identification of nonlinear systems in the time domain.²⁰ In particular, the fast and adaptive variant presented by Thirumalaisamy and Ansell³⁵ of the MEMD algorithm proposed by Rehman and Mandic²¹ was employed to extract the IMFs from the input multivariate dataset, and the HT was used to obtain the reference parameters for comparison, that is, instantaneous frequencies and amplitudes. The MEMD was applied to the set of four structural responses collected during the seismic excitation at the different levels of the numerical benchmark, aiming to identify a maximum of 10 IMFs. The IMFs were extracted considering a sifting tolerance of 0.01 (i.e., the sifting procedure is stopped when the mean-squared error between the IMFs obtained in current and in the previous iteration is lower than 0.01). It was also noted that by further decreasing the tolerance, the results did not vary and thus the outcomes of this application do not depend on the selected parameters. In the algorithm by Thirumalaisamy and Ansell,³⁵ two order-statistic filters are applied to calculate the envelopes for sifting, avoiding spline interpolation, which may become burdensome in multivariate applications. Another parameter of the algorithm is thus the window size for order-statistic filters, which is determined, for each iteration, as the median of distances between consecutive local extrema of the signal (minima or maxima) in this application.

In Figure 9, both the instantaneous frequencies obtained through the procedure presented in this paper and those obtained using the HHT are reported, superimposed on the theoretical values of the instantaneous frequencies obtained using the numerical model shown above. In particular, the instantaneous frequencies of the numerical benchmark during the seismic event are reported in blue (from light to dark blue referring to modes from 1 to 4, respectively) over time. The

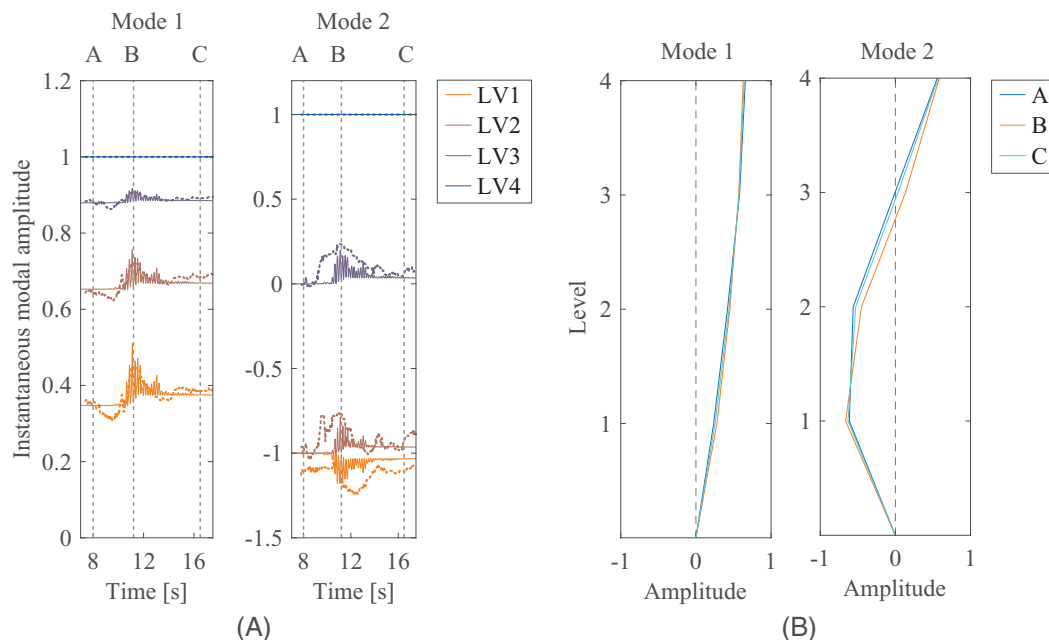


FIGURE 10 Instantaneous amplitudes of the first two modes (A) and instantaneous mode shapes at the inspection samples (B)

solid lines indicate the theoretical values, calculated by resolving the eigenproblem of the system at each time instant, considering varying stiffness. On the other hand, the dashed lines with the same color of theoretical curves represent the instantaneous identified values. Due to the application of a noise-assisted procedure, which involves the introduction of stationary noise components, the NMRs extracted through clustering, and thus the dashed lines illustrated in Figure 9, have a length limited to the regions where the signal has high amplitudes. However, these results are enough for S^2HM if the DSF is evaluated in the instant of the maximum nonlinear excursion. The orange lines in Figure 9 indicate the instantaneous frequencies of the IMFs identified by applying the MEMD to the multivariate structural response. To improve the readability of the diagrams, a median filter over 101 samples was used on all the identified parameters, that is, at each time instant, the instantaneous frequency estimate is assumed as the median value computed on a window of 101 samples centered in the considered instant. In the figure, a good agreement of the parameters identified through the proposed procedure with the theoretical curves is observable (blue lines) for the first three modes. In particular, in the instant of maximum excursion in the nonlinear field, indicated as condition B using a vertical dashed line, an accurate estimate of natural frequency is achieved for all modes. On the other hand, the instantaneous frequencies obtained through the HHT (orange lines) follow the theoretical curves only for the first two modes, showing to have no physical meaning at lower frequencies.

Figure 10A shows the instantaneous amplitude of the first two modes, computed through the HT of the reconstructed NMRs. The shapes formed of these amplitudes are referred to as “mode shapes” since they are ODSs evaluated at the resonant frequencies and are, therefore, an estimate of the instantaneous mode shapes of the structure. Moreover, in Figure 10B, three instantaneous conditions, namely, A, B, and C, corresponding to the instants prior, during (i.e., at the instant of peak response acceleration), and after the seismic strong motion, are analyzed in detail. It should be noted that, as supposed in the theoretical description of the presented approach, in this case, the fluctuations of mode shapes due to nonlinearities are generally modest compared to their mean values. Therefore, the spurious components due to nonlinearities do not affect the accuracy of the method. Indeed, the identified instantaneous mode shapes well approximate the theoretical values, especially in condition B.

The instantaneous estimates of natural frequencies and mode shapes identified in conditions A, B, and C were used to generate the uniform load line (ULL) corresponding to each condition. In particular, using p natural frequencies and mass-normalized modal vectors, an approximation of the structural flexibility matrix \mathbf{F} is evaluated as:

$$\mathbf{F} \cong \sum_{j=1}^p \frac{1}{\omega_j^2} \bar{\boldsymbol{\phi}}_j \bar{\boldsymbol{\phi}}_j^T, \quad (14)$$

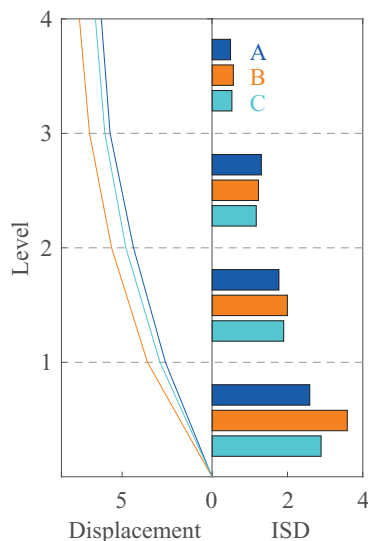


FIGURE 11 Uniform load lines and interstory drifts at the inspection samples

where $\bar{\phi}_j$ is the j -th mass-normalized modal vector. The displacements generated by the application of a unit load vector $\mathbf{p} = [1, 1, \dots, 1]^T$ are the elements of the vector:

$$\mathbf{u} = \mathbf{F}\mathbf{p} \quad (15)$$

In general, \mathbf{u} is known as the uniform load surface,³⁶ which in this case degenerates into a line. In this study, $\bar{\phi}_j$ were normalized to the identity matrix, which is proportional to the mass matrix of the system. In Figure 11, the ULL and the interstory drifts (ISDs) obtained from this analysis are reported.

As expected, the ISD in condition B is generally higher, especially for the base level. On the other hand, keeping in mind the curves of Figure 6, conditions A and C should have similar ISDs for all the levels except for the first, where a residual stiffness loss of 10% was simulated.

3.2 | Case study 2: experimental benchmark

The second case study considered in this paper is a five-story RC building tested on a shaking table at the University of California, San Diego, through the George E. Brown Jr. Network for Earthquake Engineering Simulation program (NEES-UCSD) between May 2011 and May 2012. The plan dimensions were 6.60×11.00 m and the total height was 21.34 m, with a floor-to-floor distance of 4.27 m. The shaking was impressed in the longitudinal (east-west) direction, in which the building had two RC frames as a lateral-load resisting system. The beams had a cross-section of 0.30×0.71 m, with varying connection details, and the floor system consisted of a 0.2 m thick concrete slab on all levels. More details about the specimen can be found in technical reports^{37–40} and a schematic representation of the geometry is reported in Figure 12.

Dense sensor equipment was originally deployed on the structure. In this study, only five acceleration channels were considered (S1–S5), positioned in the northern-eastern quadrant of the plant, at the floor level, in the direction of the seismic motion, as illustrated in Figure 12. Moreover, displacement measurements collected through linear (N1–N3) and string (B1–B2) potentiometers are used as reference for damage identification in this study. Detailed information on the sensor setup can be found in technical reports.^{37–40} In particular, the linear potentiometers measure the diagonal elongation of three beam-column nodes, while the string devices are used to estimate of the rotation at the base of the eastern column, calculated as:

$$\vartheta = \frac{\Delta_{B1} - \Delta_{B2}}{d}, \quad (16)$$

where Δ_{B1} and Δ_{B2} are the displacements collected by the two sensors, while d is the distance between them.

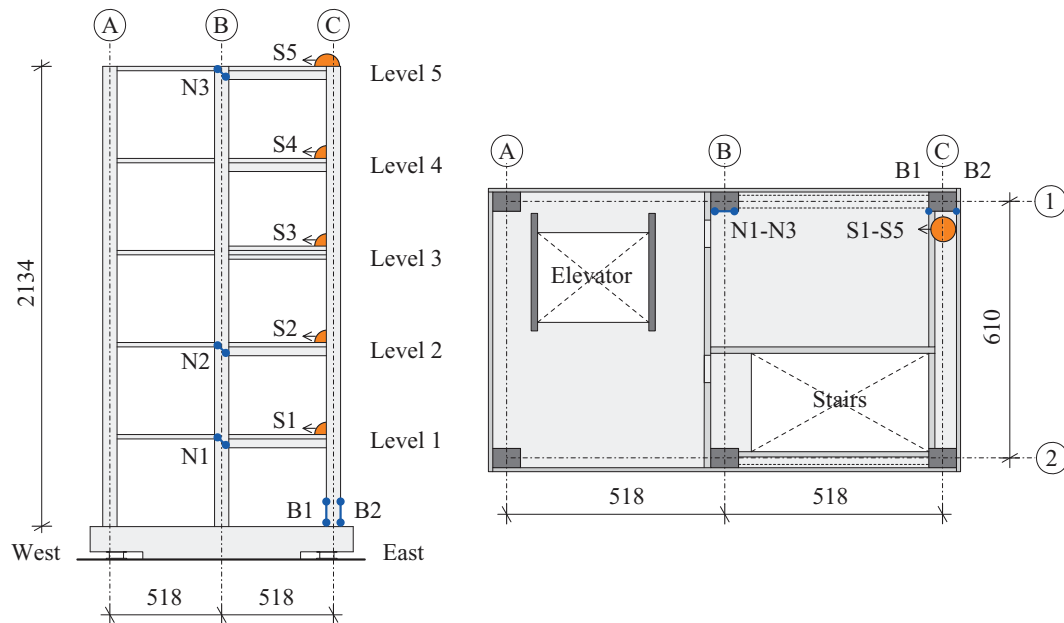
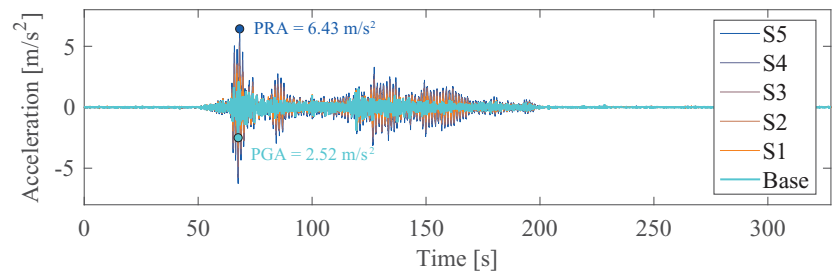


FIGURE 12 Lateral and plant scheme of the specimen, adapted from literature³⁷; dimensions in centimeters

FIGURE 13 Structural responses of the experimental case study



In the original testing campaign, the structure was first subjected to seven seismic motions with functioning base isolator devices and then tested with six seismic motions with increasing intensity with the basement of the building fixed to the shaking table. The acceleration time histories used in this study (Figure 13) were collected during the fourth test performed using the 2007 Pisco earthquake (Ica station, Peru) as input excitation with fixed-base configuration. The original sampling frequency was of 200 Hz, downsampled at 50 Hz in this study. The total duration of the recording is 327.68s.

As described in the reports of the experimental campaign,³⁷ the building was designed to reach its performance targets during the fifth seismic motion with the fixed-base configuration. Indeed, minimal damage was observed following the first two motions, with the structure remaining serviceable. Limited structural cracking was also observed following the application of the fourth motion, especially at the bases of the first-floor columns and in the slab of the first level.

The multivariate signal collected from sensors S1–S5 was used to generate the MAD through a noise-assisted procedure similar to that applied in the first case study (Figure 14A), using a threshold value of $\eta = 0.5$. The MAD was thus employed to extract the ODSs which are then clustered through SOM and k-means. As in the previous analysis, four clusters were selected, obtaining the distribution illustrated in Figure 14B.

The instantaneous natural frequencies identified through the procedure proposed in this paper and those obtained by means of the HHT are shown in Figure 15A, superimposed on the spectrogram evaluated through the short-time Fourier transform of the structural responses collected by sensor S5. The implementation features of the HHT and the approach for selecting the window size of order-statistic features are the same used for Case study 1. A median filter of 501 samples was used to improve the readability of the figure. It is possible to notice that the instantaneous frequencies obtained by the method proposed better approximate the ridges of the spectrogram, especially for the first three modes. Although the performances of HHT are higher than in the previous analysis, nonphysical IMFs are extracted at low frequencies.

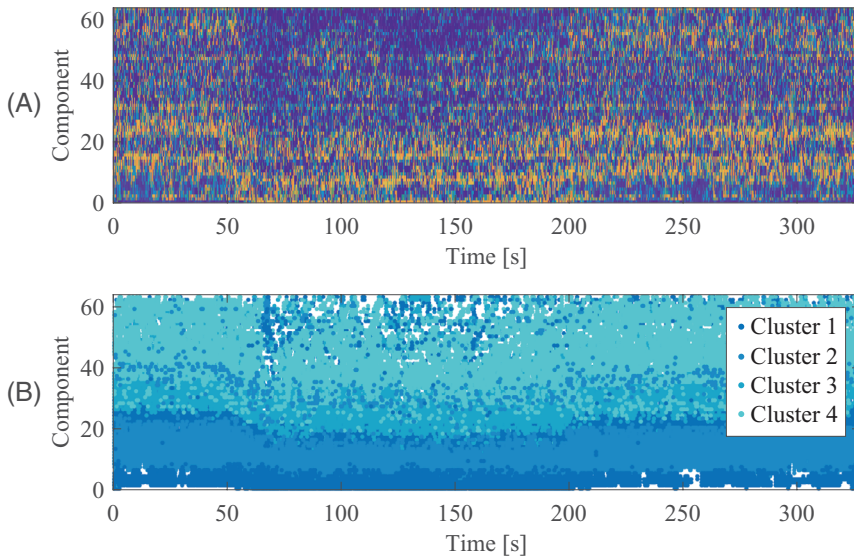


FIGURE 14 Modal assurance distribution (A) and extracted clusters (B) of the experimental case study

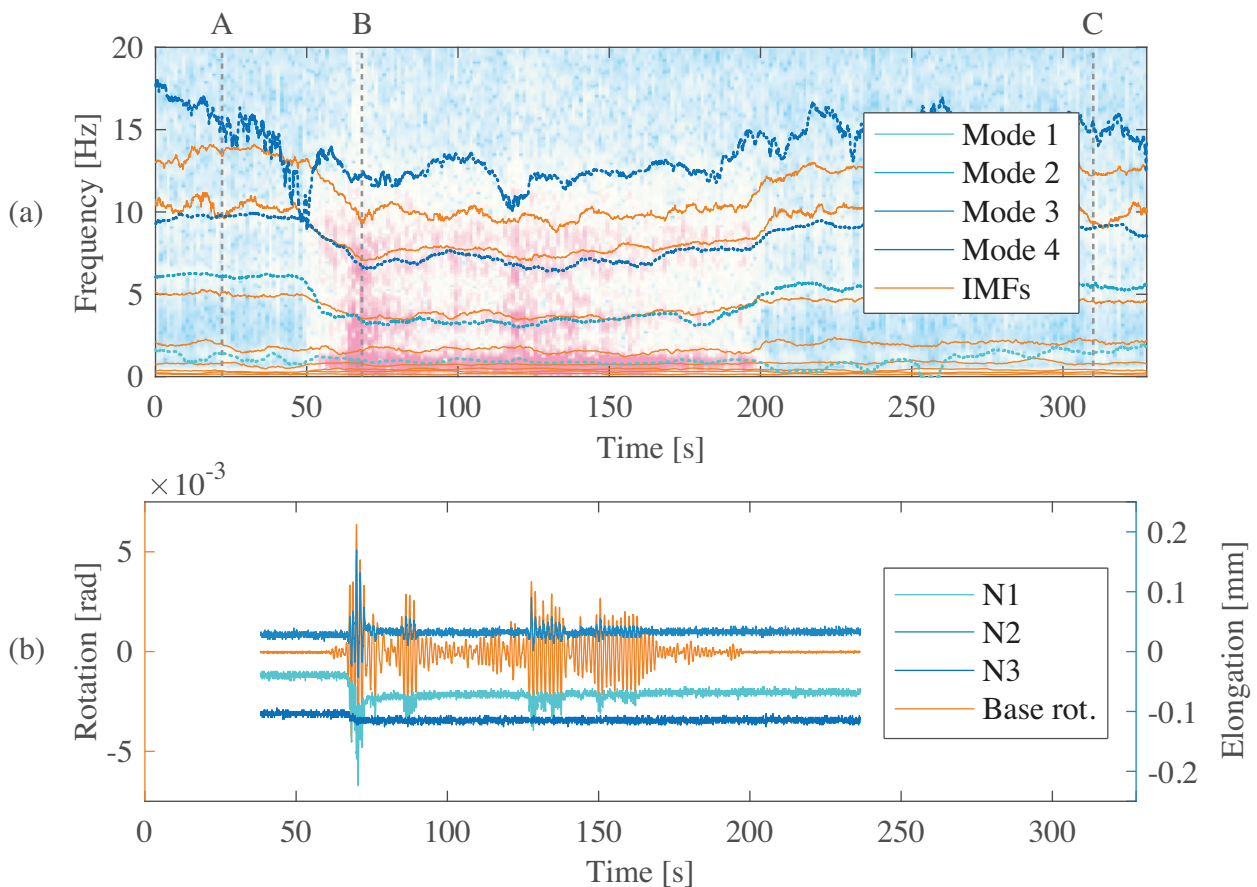


FIGURE 15 Instantaneous identified natural frequencies (A) and recordings of the potentiometers (B)

Observing the reference measurements obtained from potentiometers (Figure 15B), it is possible to notice that local minima in the identified frequencies are close to the point where maximum diagonal elongation is recorded at the nodes. In this instant, nonlinear effects can be observed since a residual displacement is present in sensor N1.

The inspection instants A, B, and C indicated in Figure 15 were considered to evaluate the first four mode shapes and the corresponding ULLs before, during, and after the seismic strong motion. In particular, condition B was selected at the instant of peak response acceleration, which is in the proximity of a local minimum of the instantaneous natural

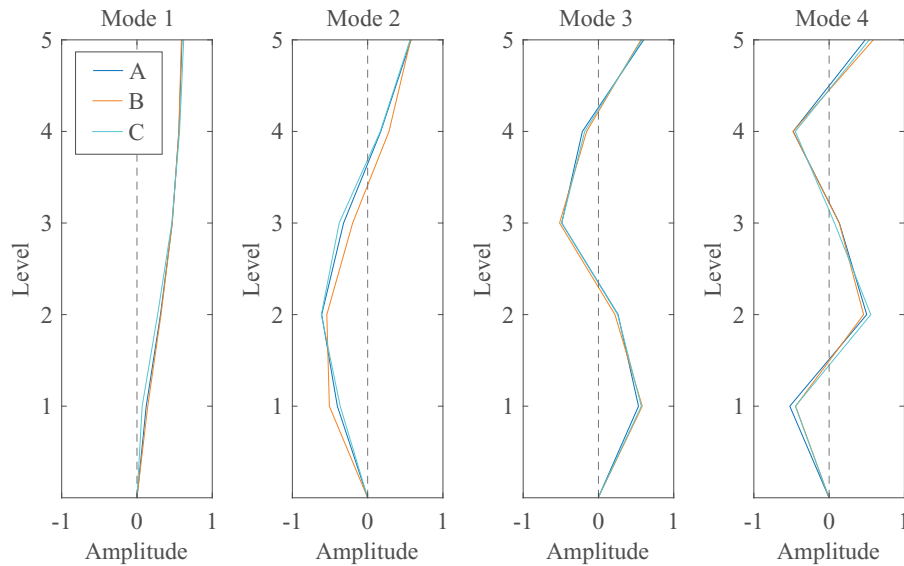


FIGURE 16 First four instantaneous mode shapes at the inspection samples

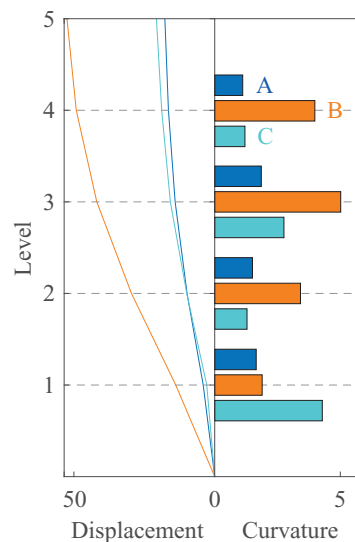


FIGURE 17 Uniform load lines and their curvature values at the inspection samples

frequencies. Observing the modal amplitudes of these three conditions in Figure 16, it is possible to notice a slight variation, which confirms the applicability of the method since the oscillation due to nonlinearities is generally modest compared to the average value. Nevertheless, the accurate estimation of such small variations enables the application of a flexibility-based method for damage detection and localization.

In Figure 17, the ULLs of the building corresponding to the inspection time instants A, B, and C are shown. Since information about the structural masses is missing, mode shapes were normalized to an identity matrix, assuming a uniform distribution along with the height of the building. Moreover, since the structural behavior may be far from the shear-type approximation, the curvature of ULL is used as a DSF in this case. A general increment in curvature is registered for each level in condition B, while after the seismic motion, only the first level has a residual difference in curvature, in agreement with the damage observed during the visual inspections.³⁸ Although the deformation of beam-column nodes is not the only effect that may affect the curvature of the ULL, this result is also confirmed by the recording of sensor N1 (Figure 15B), where clear residual elongation can be noticed.

Moreover, the rotation at the base of the structure in condition B is visibly higher than pre- and after-earthquake conditions, highlighting the presence of breathing cracks at the base of the first level columns, also confirmed by the visual

inspections. Considerable rotation at the base of the building is also recorded by the reference potentiometers B1–B2, as shown in Figure 15B.

4 | CONCLUSIONS

In this paper, a novel procedure for the identification of instantaneous dynamic parameters is presented. The MAD is used to extract the signal features which are then processed by means of an SOM and clustered through the k-means algorithm. The dimensionality reduction allows the user to consciously select the number of clusters and enables the automatization of the process employing image processing techniques. Moreover, the use of SWPT for the construction of the filter banks at the basis of MAD enables its application to short and strongly nonstationary recordings, making the procedure suitable for S²HM applications. Indeed, accurate estimates of the instantaneous modal parameters are identified, in accordance with the analytical results and comparable to the values obtained by means of other widely used procedures. Nevertheless, the main advantages over literature techniques lie in the immunity to mode mixing issues and the ability to identify vanishing components. Moreover, compared to the traditional TFRs, the MAD is not directly dependent on the amplitude of wavelet components, thus resulting in a distribution that is not generally dependent on the nature of the exciting input. This aspect is of the utmost importance when dealing with seismic excitation.

The method proposed can thus be applied to analyze the structural behavior during seismic events and investigate the condition of maximum excursion in the nonlinear field, which may include valuable information about the ongoing damage. Indeed, from the analysis of two case studies, the first consisting of a numerical model and the second involving a real-scale experimental benchmark, interesting information emerged analyzing the modal parameters at the instant of the maximum nonlinear excursion.

The results obtained using the method proposed are compared to the instantaneous parameters identified through a multivariate version of the largely used HHT, showing superior performance that enables an accurate damage identification through a flexibility-based approach. In particular, in this study, the ISDs and the curvature of the ULLs were analyzed to detect and localize the damage, showing good agreement with the theoretical results, visual inspections, and displacement recordings.

ACKNOWLEDGMENTS

The authors would like to gratefully acknowledge the availability of data recorded on the UCSD building.


DATA AVAILABILITY STATEMENT

The data that support the findings of this study for the Case study 1 are available from the corresponding author upon reasonable request. The data that support the findings of this study for the Case study 2 are openly available in the DEEDS Datasets at <http://doi.org/10.7277/D5XQ-8068>, reference number NEES-2009-0722.

ORCID

Said Quqa  <https://orcid.org/0000-0001-6388-370X>

Luca Landi  <https://orcid.org/0000-0001-7259-1186>

Pier Paolo Diotallevi  <https://orcid.org/0000-0001-5118-1700>

REFERENCES

1. Kerschen G, Peeters M, Golinval JC, Vakakis AF. Nonlinear normal modes, Part I: a useful framework for the structural dynamicist. *Mech Syst Sig Process*. 2009;23(1):170-194.
2. Ghahari SF, Abazarsa F, Taciroglu E. *Identification of Soil-Structure Systems*. Springer Tracts in Civil Engineering. 2019:139-167.
3. Kerschen G, Worden K, Vakakis AF, Golinval JC. Past, present and future of nonlinear system identification in structural dynamics. *Mech Syst Sig Process*. 2006;20(3):505-592.
4. Lin RM, Ng TY. Applications of higher-order frequency response functions to the detection and damage assessment of general structural systems with breathing cracks. *Int J Mech Sci*. 2018;148:652-666.
5. Brincker R, Ventura CE. *Introduction to Operational Modal Analysis*. John Wiley and Sons, Ltd; 2015.
6. Limongelli MP, Çelebi M. *Seismic Structural Health Monitoring. From Theory to Successful Applications*. 2019.
7. Ditommaso R, Ponzo FC, Auletta G. Damage detection on framed structures: modal curvature evaluation using stockwell transform under seismic excitation. *Earthquake Eng Eng Vib*. 2015;14(2):265-274.

8. Fu Y, Hoang T, Mechitov K, Kim JR, Zhang D, Spencer BF. Sudden event monitoring of civil infrastructure using demand-based wireless smart sensors. *Sensors (Switzerland)*. 2018;18(12).
9. Noël JP, Kerschen G. Nonlinear system identification in structural dynamics: 10 more years of progress. *Mech Syst Sig Process*. 2017;83:2-35.
10. Rosenberg RM. On nonlinear vibrations of systems with many degrees of freedom. *Adv Appl Mech*. 1966;9(C):155-242.
11. Kerschen G, Vakakis AF, Lee YS, McFarland DM, Bergman LA. Toward a fundamental understanding of the Hilbert–Huang transform in nonlinear structural dynamics. *J Vib Control*. 2008;14(1-2):77-105.
12. Pai PF, Palazotto AN. Detection and identification of nonlinearities by amplitude and frequency modulation analysis. *Mech Syst Sig Process*. 2008;22(5):1107-1132.
13. Staszewski WJ. Analysis of non-linear systems using wavelets. *Proc Inst Mech Eng Part C J Mech Eng Sci*. 2000;214(11):1339-1353.
14. De Roeck G. Model-Based Methods of Damage Identification of Structures Under Seismic Excitation. Springer Tracts in Civil Engineering. 2019:237-259.
15. Ebrahimian H, Astroza R, Conte JP, Papadimitriou C. Bayesian optimal estimation for output-only nonlinear system and damage identification of civil structures. *Struct Control Health Monit*. 2018;25(4):e2128.
16. Huang CC, Loh CH. Nonlinear identification of dynamic systems using neural networks. *Comput-Aided Civ Infrastruct Eng*. 2001;16(1):28-41.
17. Loh CH, Lin HM. Application of off-line and on-line identification techniques to building seismic response data. *Earthquake Eng Struct Dyn*. 1996;25(3):269-290.
18. Bhowmik B, Tripura T, Hazra B, Pakrashi V. Real time structural modal identification using recursive canonical correlation analysis and application towards online structural damage detection. *J Sound Vib*. 2020;468:115101.
19. Huang NE, Shen Z, Long SR, et al. The empirical mode decomposition and the Hubert spectrum for nonlinear and non-stationary time series analysis. *Proc R Soc A Math Phys Eng Sci*. 1998;454(1971):903-995.
20. Sracic MW, Allen MS. Identifying parameters of multi-degree-of-freedom nonlinear structural dynamic systems using linear time periodic approximations. *Mech Syst Sig Process*. 2014;46(2):325-343.
21. Rehman N, Mandic DP. Multivariate empirical mode decomposition. *Proc R Soc A Math Phys Eng Sci*. 2010;466(2117):1291-1302.
22. Wu Z, Huang NE. Ensemble empirical mode decomposition: a noise-assisted data analysis method. *Adv Adapt Data Anal*. 2009;1(1):1-41.
23. Ditommaso R, Mucciarelli M, Ponzio FC. Analysis of non-stationary structural systems by using a band-variable filter. *Bull Earthquake Eng*. 2012;10(3):895-911.
24. Iacovino C, Ditommaso R, Ponzio FC, Limongelli MP. The interpolation evolution method for damage localization in structures under seismic excitation. *Earthquake Eng Struct Dyn*. 2018;47(10):2117-2136.
25. Quqa S, Landi L, Diotallevi PP. Modal assurance distribution of multivariate signals for modal identification of time-varying dynamic systems. *Mech Syst Sig Process*. 2021;148:107136.
26. Mallat SG. *A Wavelet Tour of Signal Processing*. Academic Press; 2009.
27. Vetterli M, Kovačević J. *Wavelets and Subband Coding*. Prentice-Hall; 1995.
28. Quqa S, Landi L, Diotallevi PP. Instantaneous modal identification under varying structural characteristics: a decentralized algorithm. *Mech Syst Sig Process*. 2020;142:106750.
29. Serra J. *Image Analysis and Mathematical Morphology*. London: Academic Press; 1983.
30. Jain AK. Data clustering: 50 years beyond K-means. *Pattern Recognit Lett*. 2010;31(8):651-666.
31. Kohonen T. Self-organized formation of topologically correct feature maps. *Biol Cybern*. 1982;43(1):59-69.
32. Kohonen T. Essentials of the self-organizing map. *Neural Netw*. 2013;37:52-65.
33. Vesanto J, Alhoniemi E, Member S. Clustering of the self-organizing map. *IEEE Trans Neural Netw*. 2000;11(3):586-600.
34. Ester M, Kriegel HP, Sander J, Xu X. Density-connected sets and their application for trend detection in spatial databases. Proceedings of the 3rd International Conference on Knowledge Discovery and Data Mining, Newport Beach, CA; 1997:10-15.
35. Thirumalaisamy MR, Ansell PJ. Fast and adaptive empirical mode decomposition for multidimensional, multivariate signals. *IEEE Signal Process Lett*. 2018;25(10):1550-1554.
36. Zhang Z, Aktan AE. Application of modal flexibility and its derivatives in structural identification. *Res Nondestr Eval*. 1998;10(1):43-61.
37. Chen M, Pantoli E, Wang X, et al. *BNCs Report #1: Full-Scale Structural and Nonstructural Building System Performance During Earthquakes and Post-Earthquake Fire – Specimen Design, Construction, and Test Protocol*. 2013.
38. Pantoli E, Chen M, Wang X, et al. *BNCs Report #2: Full-Scale Structural and Nonstructural Building System Performance During Earthquakes and Post-Earthquake Fire - Test Results*. 2013.
39. Pantoli E, Chen M, Hutchinson T, Restrepo J. *BNCs Report #3: Full-Scale Structural and Nonstructural Building System Performance During Earthquakes and Post-Earthquake Fire - Camera and Analog Sensor Details*. 2013.
40. Chen M, Pantoli E, Wang X, Mintz S, Hutchinson T, Restrepo J. *BNCs Report #4: Full-Scale Structural and Nonstructural Building System Performance During Earthquakes and Post-Earthquake Fire - Construction Details and Technical Specifications of Specific Subsystems*. 2013.

How to cite this article: Quqa S, Landi L, Diotallevi PP. Seismic structural health monitoring using the modal assurance distribution. *Earthquake Engng Struct Dyn*. 2021;50:2379–2397. <https://doi.org/10.1002/eqe.3451>